Available online at www.sciencedirect.com
ScienceDirect
Journal of the European Ceramic Society 30 (2010) 1841–1851
www.elsevier.com/locate/jeurceramsoc

Effect of firing temperature and atmosphere on ceramics made of NW Peloponnese clay sediments. Part I: Reaction paths, crystalline phases, microstructure and colour

C. Rathossi [a], Y. Pontikes [b,c,*]

[a] Section of Earth Materials, Dept. of Geology, University of Patras, 26500 Rio, Greece
[b] Laboratory of Materials and Metallurgy, Dept. of Chemical Engineering, University of Patras, 26500 Rio, Greece
[c] Department of Metallurgy and Materials Engineering, Katholieke Universiteit Leuven, 3001 Leuven, Belgium

Available online 12 March 2010

Abstract

Archaeometric investigation on ancient ceramic collected from excavations in NW Peloponnese demonstrated that the ancient potters used the local Plio-Pleistocene clay sedimentary deposits for a large historical period. Three representative raw materials of these local sediments were chosen for experimental work aiming to evaluate their firing behaviour in a propane-fired kiln, with a different atmosphere and temperature. The determination of mineralogy and microstructure was carried out by XRD and SEM-EDS analysis. For ceramics fired at 850 and 950 °C, no significant mineralogical and microstructural differences were observed between the oxidising and reducing atmosphere. The main pyrometamorphic phases are fassaite, gehlenite, anorthite and wollastonite. On the contrary, at 1050 °C in reducing atmosphere, gehlenite and wollastonite are diminished whereas the content of anorthite, fassaite and amorphous phase is higher. The higher vitrification is attributed to Fe^{2+} that participates either in the formation of eutectic phases or in low melting crystalline phases.

Keywords: Firing; Microstructure-final; Clays; Traditional ceramics; Archaeometry

1. Introduction

The study of the macroscopic and microscopic characteristics of ancient ceramic sherds may be very helpful enabling a deeper understating of – among others – the provenance, the dating, as well as the ceramic processing followed by the potters of the time. The analysis on non-glazed sherds typically involves a number of complementary techniques, such as colour determination for both the surface and the core, major, minor and trace element analysis, crystalline/amorphous phase analysis, study of the microstructure by optical and electron microscopy (scanning, cathode-luminescence and transmission), Mössbauer spectroscopy and more.

Provided the above analyses have permitted the identification of the clay deposits used and the assessment of the ceramic processing employed, it is expected as a final step to reproduce the ceramic sherd by achieving a material with comparable micro and macro characteristics as that produced by the potters of the time. A number of works are devoted in such a reproduction process and in the study of the pathways of clay firing, however, results mainly derive from ceramics fired in resistance (i.e. muffle/electric) furnaces in oxidising atmosphere.[1–9] Nonetheless, ancient Greek ceramics have been fired under both oxidising and reducing conditions (e.g. [10,11]), and the same applies to non-Greek potteries as well.[4,12] Despite the great interest in this field, a relatively small number of works are devoted to the study of firing in reducing conditions,[13–17] which is counterbalanced by a substantial interest in the technical literature.[18,19]

To assess the effect of firing conditions on the mineralogy and microstructure of clay-based ceramics, and therefore provide direct comparison between contemporary and ancient bodies, ceramics were fired in oxidising and reducing atmospheres in a propane-fired kiln. Raw materials were collected from local Plio-Pleistocene sediments, close to Patras, prefecture of Achaia, NW Peloponnese. Excavations in this region give evidence of activity of ceramic manufacturing during Archaic (6th c. B.C.), Hellenistic (3rd c. B.C.) and Roman (1st–3rd c. A.D.) period.[20] Previous research on collected fine wares has led to the conclusion that

* Corresponding author at: Department of Metallurgy and Materials Engineering, Katholieke Universiteit Leuven, 3001 Leuven, Belgium.
Tel.: +32 16320392; fax: +32 16321991.
E-mail address: Yiannis.Pontikes@mtm.kuleuven.be (Y. Pontikes).

0955-2219/$ – see front matter © 2010 Elsevier Ltd. All rights reserved.
doi:10.1016/j.jeurceramsoc.2010.02.002

the artefacts have been most probably produced from the clay sediments used in this study. This is supported by a number of findings, such as the mineralogy and particle size distribution and most notably the geochemistry between ceramics and clay sediments.[21–23]

The goal of this study is to provide a set of results that would assist during the interpretation of ancient ceramic sherds and find application in the contemporary ceramic industry. An extended micro-chemical analysis on the crystalline phases as well as a comparison between the microstructures produced here with the ancient ceramic sherds is presented in Part II.[24]

2. Experimental

The three raw materials used in the experiments, G, TS and TH, have been collected from the region of Patras. Details concerning the sampling location and their geological context are provided elsewhere.[21,23] Analysis on the methods employed for the chemical and mineralogical analysis is also provided in the previously cited work. The organic content has been determined by pyrolysis at 400 °C for 16 h.[25] The particle size distribution has been measured by laser scattering (Hydro 2000M, Malvern, U.K.).

For the preparation of the specimens, the raw materials were gently crushed by hand in an agate mortar, without any refinement. The powder was mixed with water and the plastic mass was shaped by hand in discs, of 5 cm dia. by 1.5 cm height, approximately. After drying at room temperature for five days, the discs were placed in a resistance oven at 50 °C for 24 h.

Firing was performed in a propane-fired kiln. Propane combustion results in different products, depending on oxygen ratio and temperature, the main compounds being hydrocarbons, carbonyl compounds, alcohols and organic acids.[26] The higher concentrations, besides CO_2 and CO, apply for propane, methane, ethylene, acetylene, propylene and ethane.[26] Ancient potters used for fuel wood, olive pits, and plants such as vine cuttings, straw, pistachio shells, almond shells or prickly shrubs.[27] The combustion of those organic materials releases CO_2, CO and other volatile and semi-volatile emissions. Again, the specific products depend on the oxygen ratio and temperature, however, for the case of pyrolysis and combustion of olive-oil solid waste as an example, the main products are methane, ethylene, acetylene, as well as, propane, propene, benzene, etc.[28] The similarity found between the products in the firing atmospheres supports the choice of propane as a firing medium for archaeometric study.

The heating and cooling rate was in all cases 3 °C min^{-1}, the firing temperature was 850, 950 and 1050 °C and the soaking time was 1 h. Eighteen experiments were conducted; for each sample, three firing temperatures, in oxidising and reducing atmosphere, were tested. The firing atmosphere was controlled by regulating the primary and secondary air flow; Bernoulli-type burners were used. Firing initiated in oxidising atmosphere and the transition to a reducing atmosphere, where applicable, took place for $T > 800$ °C and throughout the soaking period. During cooling, the settings for the burners were not modified initially, however, for $T < 800$ °C the atmosphere was inverted to oxidising as there was no practical effect on reduction. The measurement of the firing atmosphere was performed using a flue gas analyser employing electrochemical cells, measuring O_2 and CO and calculating CO_2 (Testo 335, Germany). A sample of hematite powder was placed next to the clay body during the firing tests in order to be used as diagnostic for the specific firing conditions. The colour of the green (unfired) and fired bodies was determined by comparison to the Munsell soil chart.

Analysis of the crystalline phases after firing was performed by X-ray diffraction (Bruker D8 Advance, USA) equipped with a LynxEye® detector. The scanning area covered the 2θ interval 2–70°, with a scanning angle step of 0.015° and a time step of 0.3 s. Qualitative analysis was performed by the DIFFRACplus EVA® software (Bruker-AXS, USA) based on the ICDD Powder Diffraction File. The mineral phases were quantified using a Rietveld-based quantification routine with the TOPAS® software (DIFFRACplus TOPAS Ver. 3.0 Tutorial, Bruker-AXS, USA). The routine is based on the calculation of a single mineral-phase pattern according to the crystalline structure of the respective mineral, and the refinement of the pattern using a non-linear least squares routine. A number of corrections of various parameters including, among others, the instrument's geometry, background, sample displacement, detector type, mass absorption coefficients of the refined phases and the preferred orientation of certain $h\,k\,l$ planes were also applied in order to achieve the optimum pattern fitting. A new scaling factor and crystallite size was then calculated for each mineral phase enabling the calculation of the mineral content in the sample.[29] The quantification errors were also calculated for each phase as a weight percent of the crystalline phases. Additionally, the R_{wp} (R—weighted pattern) and R_{exp} (R—expected pattern) parameters were calculated in order to check the fit accuracy, following the "Goodness Of Fit" (GOF) or chi^2 rule, where the more the R_{wp} to R_{exp} ratio approaches the value of 1 the better is the fitting of the refinement.[29] The amorphous phase was calculated by the determination of the degree of crystallinity. The method combines Rietveld refinement and single line fitting, where the single peak describes the amorphous phase intensity. The results obtained from this quantification method are expressed as weight percent of the crystalline phases of the sample and should be regarded as relative and not absolute. The microstructure and micro-chemical analysis of the samples was performed on thin sections, using Scanning Electron Microscopy (JEOL 6300, Japan) fitted with an Energy Dispersive X-ray Spectrometer (LINK PentaFET 6699, Oxford Instruments, U.K.), respectively. The samples were embedded in cold epoxy resin, polished gradually with SiC papers up to 2400 grit and were finally carbon-coated. Natural minerals and synthetic oxides were used as calibration standards.

3. Results and discussion

3.1. Raw materials

The chemical analysis of the raw materials, Table 1, reveals that Fe_2O_3, MnO, MgO, Na_2O, K_2O, TiO_2 and P_2O_5, range in comparable levels. The main difference regards the levels of SiO_2, 42.03–51.17 wt%, Al_2O_3, 10.48–12.80 wt%, CaO,

Table 1
Concentration, in wt%, of the major elements of the raw materials.

	SiO_2	Al_2O_3	Fe_2O_3	MnO	MgO	CaO	Na_2O	K_2O	TiO_2	P_2O_5	LOI	Total
G	42.03	12.80	6.20	0.15	3.38	9.48	0.91	2.36	0.66	0.12	21.76	99.85
TS	51.17	12.62	5.25	0.08	2.76	10.33	1.17	2.15	0.68	0.11	14.03	100.35
TH	47.77	10.48	5.13	0.12	2.58	13.97	1.23	1.83	0.58	0.12	15.91	99.72

Table 2
Semi-quantitative, in wt%, mineralogical composition of the raw materials employed in the firing experiments. Qtz: quartz, Ab: albite, Or: orthoclase, Cc: calcite, Mi: white mica (illite/muscovite), Chl: Fe-rich chlorite, ML: mixed-layer (white mica/chlorite, chlorite/vermiculite, illite/smectite).

Location	Samples	Qtz	Ab	Or	Cc	Mi	Chl	ML
NE Patras	G	26.6	7.1	6.6	14.2	17.4	15.3	12.8
	TS	29.3	12.4	7.8	13.7	13.4	14.5	8.9
SW Patras	TH	32.5	11.1	6.2	17.4	10.7	12.3	9.8

9.48–13.97 wt% and the loss on ignition, 14.03–21.76 wt%. The content of organic material was 2.15 wt% for G, 2.10 wt% for TH and 1.88 wt% for TS.

The mineralogical analysis, Table 2, shows that the materials are composed of quartz, albite ($NaAlSi_3O_8$), orthoclase ($KAlSi_3O_8$), calcite ($CaCO_3$), white mica (illite/muscovite, $K(Al,Mg,Fe)_2(Si_3,Al)O_{10}(OH)_2$), Fe-rich chlorite ($(Mg,Fe^{2+})_5Al)((Al,Si_3)O_{10})(OH)_8$), mixed-layer clay minerals (white mica/chlorite, chlorite/vermiculite and illite/smectite). As accessory minerals, iron oxy-hydroxides, rutile, ilmenite, Cr-spinel, apatite, zircon and garnet were also detected by optical and electron microscopy.

The fraction of clay minerals is higher in G, quartz and calcite is higher in TH, whereas albite and orthoclase are higher in TS. The higher fraction of clay minerals is responsible for the increased loss on ignition of G. This is also expected to contribute to a comparably more reactive body for G. On the contrary, TS and TH have higher levels of temper materials (for the typical firing scheme employed). The higher level of calcite in TH is likely to enhance the formation of calcium-(alumino)-silicates. Apart from the effect on porosity, and therefore engineering properties related to, calcite participates in the neomineralisation of an array of crystalline phases, and affects the usable firing interval (i.e. without body deformation) as well as the thermal expansion coefficient.

The $d(10)$, $d(50)$ and $d(90)$ values, in μm, for G are: 1.65, 7.31, 80.63, for TS: 1.34, 8.87, 291.28, and for TH: 1.61, 11.07, 459.85. It is evident therefore that G has the finest particle size distribution, whereas TH has considerably more coarse particles.

3.2. Firing and fired bodies

During the firing experiments, the effort was to establish two combustion regimes: excess of air and excess of fuel (deficiency of air). Due to the Bernoulli-type burners used in the experiments (as opposed to pre-mixing burners), the bottom of the kiln enables the introduction of air in the firing chamber. Moreover, the firing atmosphere in the kiln is continuously changing according to the ignition and cease of the burners (Fig. 1). In

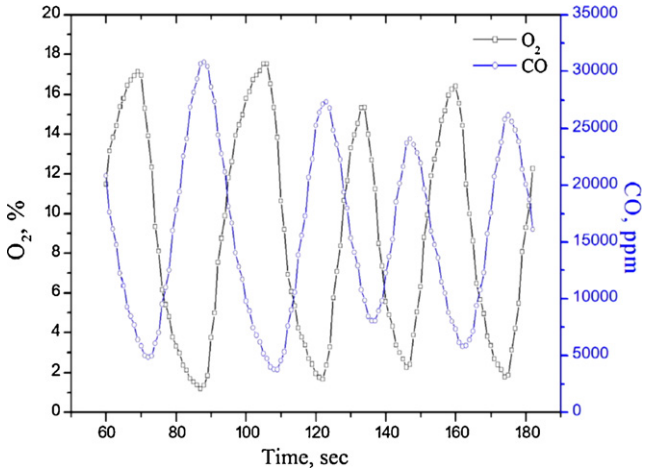

Fig. 1. Concentration of the gases O_2 and CO for reducing atmosphere at 950 °C.

view of the above, it has not been possible to achieve low levels of O_2, Table 3, which are higher than 7% approximately (average values) in all cases and increase, as expected, for oxidising firing. The above results suggest that the reducing atmosphere employed is in effect mildly reducing. This is in line with the results for the powder of hematite included in the firings, where partial reduction to magnetite was only observed for a reducing atmosphere at 1050 °C. In view of the oxidising firing up to 800 °C, it is expected that the conditions have permitted an effective oxidation (burn-out) of the organic material in the ceramic bodies and therefore the carbon content does not contribute to the reduction. The CO levels are increased in reducing atmosphere, but the absolute values in general diminish as the temperature increases. On the contrary, CO_2 levels increase as temperature rises but are comparable for a specific temperature. As a result, the ratio of CO/CO_2 is declining for increasing temperature. Finally, it should be remarked that the analysis of the firing atmosphere is not exhaustive. According to the water–gas reaction: $H_2O + CO \rightleftarrows CO_2 + H_2$, both H_2O, which enhances heat trans-

Table 3
Average values of O_2, CO, CO_2 and CO/CO_2, in %, for all firing conditions tested.

°C		O_2, %	CO, %	CO_2, %	CO/CO_2, %
850	Ox	11.70	0.26	5.91	4.40
	Rd	10.66	1.34	5.84	22.95
950	Ox	8.98	0.02	7.89	0.25
	Rd	8.56	1.10	7.39	14.88
1050	Ox	8.33	0.10	8.33	1.20
	Rd	6.98	0.96	8.54	11.24

fer, and H_2, a gas with high reduction potential and permeability in the ceramic microstructure, are expected to be constituents of the atmosphere.[13] However, there are no available data on their concentrations. More information on the products found in propane flames can be retrieved elsewhere.[26]

To assist the presentation of the data for the fired bodies and avoid the use of multiple graphs and tables, the results for the quantitative analysis are summarised in Table 4, and for the colour in Table 5.

3.2.1. Oxidising atmosphere

At 850 °C the microstructure is characterized by open, elongated and interconnected pores (Figs. 2(a) and 3(a)). The individual minerals are well defined as they retain their characteristic morphologies. The phases identified by XRD are quartz, anorthite, albite, sanidine, anorthoclase, fassaite (Fe^{3+},Al-rich clinopyroxene), gehlenite, hematite, magnetite, wollastonite, forsterite, calcite, white mica (illite/muscovite) and amorphous (Table 4). Quartz, albite, calcite and white mica (0 0 1, 1 1 0) are the remaining phases from the raw material whereas the other phases present have been formed during firing. Chlorite is no longer present.

The levels of quartz and albite are close to the original content due to the reduced reactivity in view of the low firing temperature. Indeed, both quartz and albite grains have retained the original angular morphology. A fraction of quartz is likely to have participated in the formation of the gehlenite,[30] reaction (1)

$$Al_2O_3 + SiO_2 + 2CaCO_3 \rightleftarrows Ca_2Al_2SiO_7 + 2CO_2 \quad (1)$$

Participation of quartz in the formation of the wollastonite,[7,31] reaction (2), and the anorthite,[7,30] reaction (3) is also likely, yet these new phases are present in very low concentrations at 850 °C. The crystallisation of these phases typically occurs in the surface of quartz grains, however, only reactions (1) and (2) have been verified by EDS analysis. The fine grain size of raw materials probably promotes the crystallization of anorthite at low temperature

$$CaCO_3 + SiO_2 \rightleftarrows CaSiO_3 + CO_2 \quad (2)$$

$$2Al_2O_3 + 4SiO_2 + 2CaCO_3 \rightleftarrows 2CaAl_2Si_2O_8 + 2CO_2 \quad (3)$$

The dissociation of calcite and the dehydroxylation of mica, chlorite and mixed layers have already initiated at a lower temperature and only calcite and mica are present at 850 °C in diminished quantities. As optical and electron microscopy reveal, the grains of calcite are partly decomposed whereas the grains of mica have preserved the characteristic laminar habit (Figs. 2(a) and 3(a)). However, in sample TH, partially decomposed calcite grains appear more often as a result of higher calcite quantity (CaO 13.97 wt%) and larger size (up to 200 μm). The dissociation of calcite yields CO_2 and CaO; the latter functions as mineraliser and promotes the formation of an array of neoformed phases (some already presented in reactions (1)–(3)). Mica participates in the formation of sanidine and anorthite,[32] according to reaction (4):

$$KAl_2(Si_3, Al)O_{10}(OH)_2 + CaCO_3 + 2SiO_2 \rightleftarrows KAlSi_3O_8 + CaAl_2Si_2O_8 + CO_2 + H_2O \quad (4)$$

Other reactions between mica and calcite involve, among others, the formation of sanidine and gehlenite (5) and gehlenite (6):

$$KAl_2(Si_3, Al)O_{10}(OH)_2 + 2CaCO_3 + SiO_2 \rightleftarrows Ca_2Al_2SiO_7 + KAlSi_3O_8 + 2CO_2 + H_2O \quad (5)$$

$$2KAl_2(Si_3, Al)O_{10}(OH)_2 + 6CaCO_3 \rightleftarrows 3Ca_2Al_2SiO_7 + 6CO_2 + 2H_2O + K_2O + 3SiO_2 \quad (6)$$

Chlorite participates in the formation of fassaite[33] as reaction (7) indicates:

$$(Mg, Fe^{2+})_5Al(Al, Si_3)O_{10}(OH)_8 + 4CaCO_3 + 2SiO_2 \rightleftarrows 4Ca(Mg, Fe^{2+})Si_2O_6 + (Mg, Fe)Al_2O_4 + 4CO_2 + 4H_2O \quad (7)$$

The crystallisation of fassaite also results from the reaction between mixed-layer illite/chlorite and calcite, according to reaction (8):

$$K((Fe^{3+}, Mg)_5, Al_2)(Si_5, Al_3)O_{20}(OH)_{10} + 2CaCO_3 \rightleftarrows 2Ca(Fe^{3+}, Mg)AlSiO_6 + KAlSi_3O_8 + Fe_2O_3 + MgAl_2O_4 + 2CO_2 + 5H_2O \quad (8)$$

In fact, the crystallisation of fassaite predominates that of gehlenite at 850 °C probably due to the fine particle size of raw materials, the almost homogeneous dispersion of calcite in the micromass and the content of CaO (lower than 15 wt%).

The formation of spinel, as anticipated by reactions (7) and (8) is not easy to be detected in XRD patterns, since its main reflections overlap with the reflections of minerals such as quartz and fassaite.

Besides the formation of $KAlSi_3O_8$ according to reactions (4), (5) and (8), EDS analyses point out that K-feldspar has been formed in the rims of albite grains, after substitution of Na by K (released after the dehydroxylation of illite). Magnetite results after the Fe^{2+} release from chlorite breakdown and remains for all firing temperatures tested in oxidation. The most plausible explanation has to do with the limited possibility of oxidising gases to penetrate the body. Actually, the inverse phenomenon, of hematite remaining in a reducing atmosphere, was also observed in the present work and is attributed to the same mechanism, as also reported elsewhere.[34,35] Nonetheless, a part of magnetite is expected to oxidise resulting in the formation of hematite. In addition, hematite is formed on the dehydration of iron oxy-hydroxides in the raw materials and after the dehydroxylation of illite.[36,37] The amorphous phase is mainly comprised of clay/phyllosilicate minerals after the dehydroxylation they have been subjected to and only a fraction is expected to be a glassy phase.

Table 4
Rietveld-based quantification analysis of the fired bodies G, TS and TH, in wt%, of the crystalline phases. The numbers in parentheses declare the quantification errors; n.d.: not detected; GOF: "Goodness of Fit" = $chi^2 = R_{wp}/R_{exp}$, see text for details. Abbreviations: Qtz: quartz, An: anorthite ($An_{75–100}$), Ab: albite (refers to $An_{0–15}$ content at 850 °C and $An_{0–50}$ at 950 and 1050 °C), Sa: sanidine (>Or_{44}), Ant: anorthoclase (<Or_{25}), Fs: fassaite (Fe^{3+}, Al-rich clinopyroxene), Gh: gehlenite, He: hematite, Mt: magnetite, Wo: wollastonite, Fo: forsterite, Cc: calcite, Mi: white mica.

	Temp. (°C)	Qtz	An	Ab	Sa	Ant	Fs	Gh	He	Mt	Wo	Fo	Cc	Mi	Lime	Amorphous	GOF
G																	
Ox	850	27.2(3)	1.1(4)	7.4(1)	14.7(4)	2.8(2)	7.9(1)	5.6(7)	1.7(3)	1.4(2)	1.1(3)	n.d.	2.3(4)	8.1(1)	n.d.	19.0	1.19
	950	25.6(7)	7.0(2)	11.8(1)	15.7(3)	1.1(3)	15.7(6)	8.5(4)	2.5(2)	2.1(2)	2.0(3)	2.3(5)	n.d.	n.d.	n.d.	5.8	1.20
	1050	21.2(1)	20.9(1)	9.2(1)	6.4(3)	1.0(8)	19.9(1)	3.3(3)	1.2(2)	5.0(3)	4.3(6)	3.8(7)	n.d.	n.d.	n.d.	4.0	1.13
Rd	850	26.8(2)	1.4(3)	7.5(1)	14.3(2)	2.7(2)	7.9(1)	5.7(6)	1.4(3)	1.8(2)	1.3(2)	n.d.	2.0(3)	7.8(9)	n.d.	19.5	1.18
	950	25.2(7)	8.4(1)	13.5(6)	14.1(4)	1.9(3)	15.9(7)	5.8(4)	1.1(1)	3.4(2)	2.8(4)	1.7(4)	n.d.	n.d.	n.d.	6.3	1.17
	1050	13.3(7)	27.3(2)	5.7(3)	5.3(7)	1.3(1)	24.9(1)	0.3(2)	1.0(1)	3.4(2)	2.8(2)	1.0(4)	n.d.	n.d.	n.d.	13.8	1.09
TS																	
Ox	850	30.5(1)	2.0(4)	8.0(1)	13.9(2)	0.4(6)	9.6(8)	6.6(5)	1.1(2)	1.7(2)	1.3(4)	n.d.	1.1(1)	5.8(7)	n.d.	18.0	1.17
	950	27.9(2)	5.2(3)	12.2(1)	12.7(5)	2.5(1)	13.9(1)	8.5(8)	1.2(2)	2.2(3)	6.3(9)	2.5(7)	n.d.	n.d.	n.d.	5.1	1.23
	1050	18.6(2)	16.7(4)	13.6(2)	9.8(3)	2.3(1)	16.7(1)	3.3(3)	1.1(2)	4.4(3)	5.3(6)	3.4(7)	n.d.	n.d.	n.d.	4.9	1.14
Rd	850	30.1(1)	2.7(1)	8.2(4)	12.3(5)	1.0(2)	9.7(9)	6.9(5)	1.0(2)	2.0(2)	1.3(4)	n.d	1.0(1)	5.4(7)	n.d.	18.5	1.18
	950	27.4(1)	8.1(6)	8.4(2)	14.1(2)	0.5(1)	14.2(9)	8.2(5)	1.1(2)	3.9(2)	5.6(6)	3.0(7)	n.d.	n.d.	n.d.	5.7	1.22
	1050	11.9(6)	25.1(1)	9.1(1)	4.4(3)	2.6(2)	22.9(1)	1.1(2)	0.4(1)	2.3(2)	6.5(3)	1.3(7)	n.d	n.d	n.d	12.5	1.10
TH																	
Ox	850	34.9(2)	1.4(5)	7.8(5)	7.8(3)	1.4(3)	11.5(1)	10.1(8)	1.9(2)	0.6(2)	2.8(5)	n.d.	3.0(4)	4.2(5)	0.5(1)	12.2	1.22
	950	32.0(1)	4.3(6)	5.8(5)	13.8(3)	1.9(1)	13.3(7)	13.2(6)	1.1(2)	1.7(2)	7.3(5)	1.4(6)	n.d.	0.2(3)	n.d.	4.0	1.21
	1050	21.7(4)	15.5(5)	4.5(4)	10.3(4)	1.4(3)	19.2(5)	10.8(3)	0.7(1)	2.4(1)	10.0(4)	1.4(4)	n.d.	n.d.	n.d.	2.2	1.19
Rd	850	34.3(2)	1.6(5)	8.0(7)	7.5(3)	1.2(3)	11.6(1)	10.2(8)	1.1(2)	1.2(2)	2.8(4)	n.d.	2.8(3)	4.0(5)	0.4(9)	13.3	1.22
	950	30.6(1)	5.9(2)	7.5(6)	10.3(2)	0.6(1)	13.8(8)	14.5(6)	0.8(1)	2.0(1)	7.4(5)	1.2(4)	n.d.	n.d.	n.d.	5.5	1.23
	1050	15.9(5)	16.3(5)	9.1(5)	6.4(6)	1.0(6)	25.6(9)	4.4(2)	0.7(2)	0.7(1)	7.6(5)	1.2(6)	n.d.	n.d.	n.d.	11.2	1.13

At 950 °C, the microstructure of the body is comparable with that at 850 °C (Figs. 2(b) and 3(b)) Porosity remains open and interconnected. Quartz is decreased whereas sanidine and anorthoclase (calculated together) are at the same levels except for TH. Calcite and white mica are no longer present for G and TS, however, trace of white mica is still preserved in TH (reflection 0 0 1, only detected at XRD pattern). All other phases, i.e. magnetite, gehlenite, fassaite, wollastonite and anorthite, are increased. Hematite is increased for G and TS and slightly reduced for TH. Gehlenite presents its maximum at this temperature. The higher level of albite compared with that at 850 °C is primarily attributed to the increasing contribution of An members ($An_{0–50}$) in a solution/precipitation process where the original Na-rich plagioclase is progressively dissolved with a concurrent epitactic formation of a more Ca-rich plagioclase. Forsterite is a new mineral detected; a possible route for its formation is proposed in reaction (9), which is similar to (7) since it involves chlorite and calcite[38]:

$$3(Mg, Fe^{2+})_5Al(Al, Si_3)O_{10}(OH)_8 + 2CaCO_3 \rightleftarrows 5(Mg, Fe^{2+})_2SiO_4 + 2Ca(Mg, Fe^{2+})Si_2O_6 + 3(Mg, Fe)Al_2O_4 + 2CO_2 + 12H_2O \quad (9)$$

The amorphous phase at 950 °C has decreased compared to 850 °C as the crystallisation of new minerals is enhanced.

At 1050 °C, the body is comprised of both open and closed pores and there is evident bonding between the grains (Figs. 2(c) and 3(c)). Both the pores and the grains are more rounded compared to those from a lower firing temperature. Quartz is further decreased and ranges from 18.6 wt% for TS to 21.7 wt% for TH. A coronitic rim is evident on many occasions on the grain boundaries and around pores of pre-existed calcite grains. Albite is reduced, except for TS. Sanidine + anorthoclase

Table 5
Macroscopic observation of colour for the fired bodies G, TS and TH, according to Munsell soil colour chart.

	Green body	Fired bodies			
		Atm	850 °C	950 °C	1050 °C
G	GLEY 1 5GY 4/1 dark greenish gray	Ox	7.5 YR 6/6 reddish yellow	5YR 6/6 reddish yellow	7.5YR 6/4 light brown
		Rd	7.5 YR 6/6 reddish yellow	7.5 YR 6/4 light brown	7.5YR 5/4 brown
TS	GLEY 2 5BG 6/1 greenish gray	Ox	7.5YR 6/6 reddish yellow	7.5YR 7/6 reddish yellow	7.5YR 6/4 light brown
		Rd	7.5YR 6/6 reddish yellow	7.5YR6/4 light brown	10YR 6/4 light yellowish brown
TH	2.5Y 6/2 light brownish gray	Ox	7.5YR 6/4 light brown	10YR 7/4 very pale brown	10YR 7/3 very pale brown
		Rd	7.5YR 6/4 light brown	10YR 7/4 very pale brown	5Y 7/4 pale yellow

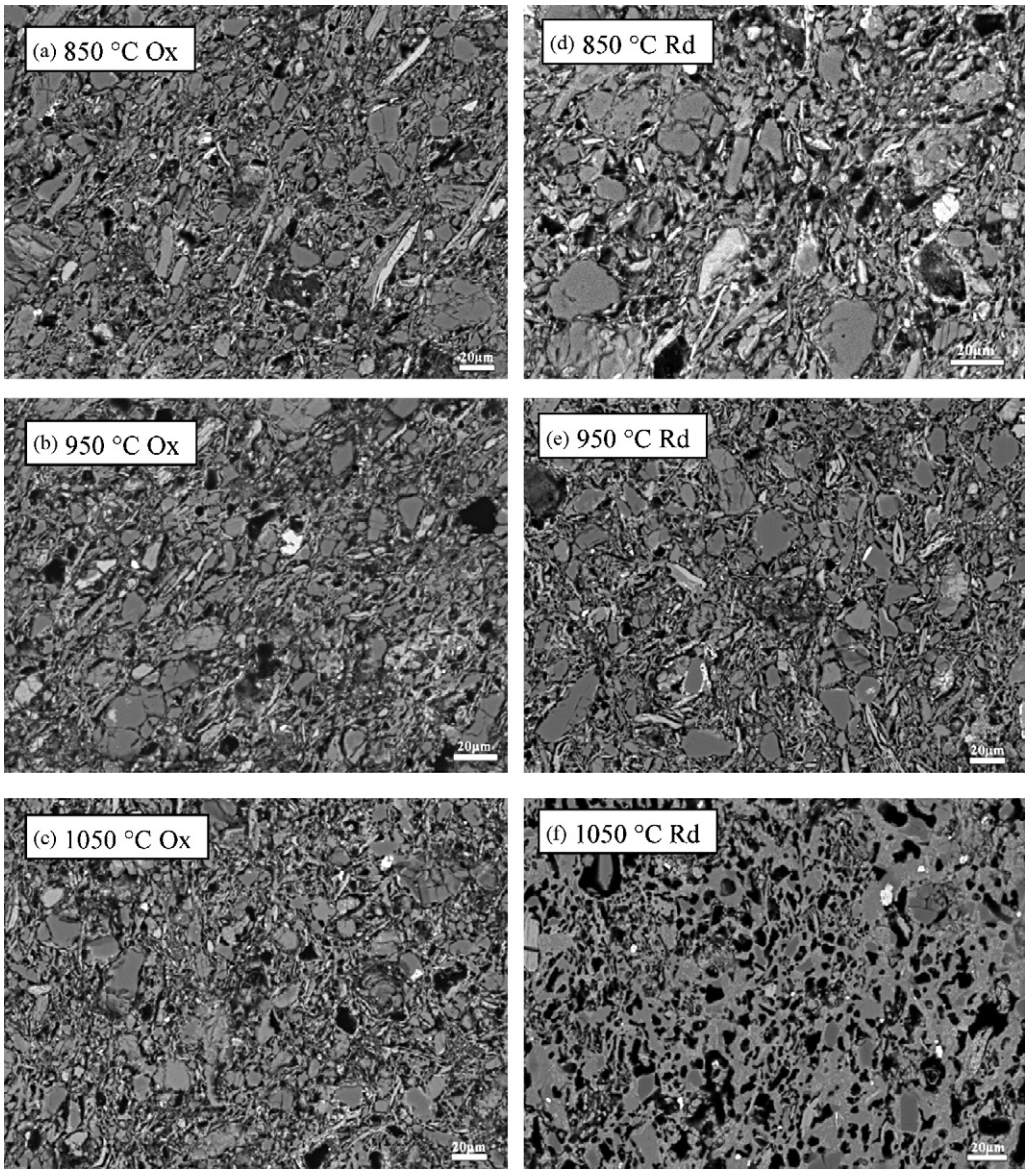

Fig. 2. Backscattered electron images of polished surfaces, after firing G body in the interval 850–1050 °C, in oxidation (a)–(c) and in reduction (d)–(f).

and gehlenite are significantly reduced in the body, whereas hematite is slightly reduced. Sanidine + anorthoclase, probably start to undergo partial melting as they attain a sponge-like appearance, whereas hematite decreases as Fe^{3+} incorporates in the structure of gehlenite and fassaite.[39–41] According to reaction (10), gehlenite reacts with quartz towards wollastonite and anorthite:

$$Ca_2Al_2SiO_7 + 2SiO_2 \rightleftarrows CaSiO_3 + CaAl_2Si_2O_8 \quad (10)$$

Apart from reaction (10), anorthite can also form after gehlenite and amorphous clay[37] after the dehydroxylation, via reaction (11):

$$Ca_2Al_2SiO_7 + 3SiO_2 + Al_2O_3 \text{ (amorphousclaysubstance)} \rightleftarrows 2CaAl_2Si_2O_8 \quad (11)$$

According to reactions (10) and (11), gehlenite behaves as an intermediate compound reacting towards anorthite and wollastonite or only anorthite. Therefore, the ratio of gehlenite/anorthite may be considered diagnostic for the attainment of a particular firing temperature.[42] For the G samples, this ratio is 5.1, 1.2 and 0.2 for 850, 950 and 1050 °C respectively. However, it should be noted, that gehlenite in solid solution with akermanite can react towards fassaite instead of anorthite, if there is availability of (Fe,Mg)-bearing amorphous phases (after the dehydroxylation of Fe-rich chlorite and illite).[37] The presence of gehlenite, observed by other authors as well,[6,7] is ascribed to the grain size of calcite, promoting micro-sites enriched in Ca.[7,43] However, the findings of our work suggest that the firing atmosphere is another parameter that has to be taken into consideration. Fassaite is increased to 16.8–19.9 wt% approximately, whereas anorthite presents a considerable increase,

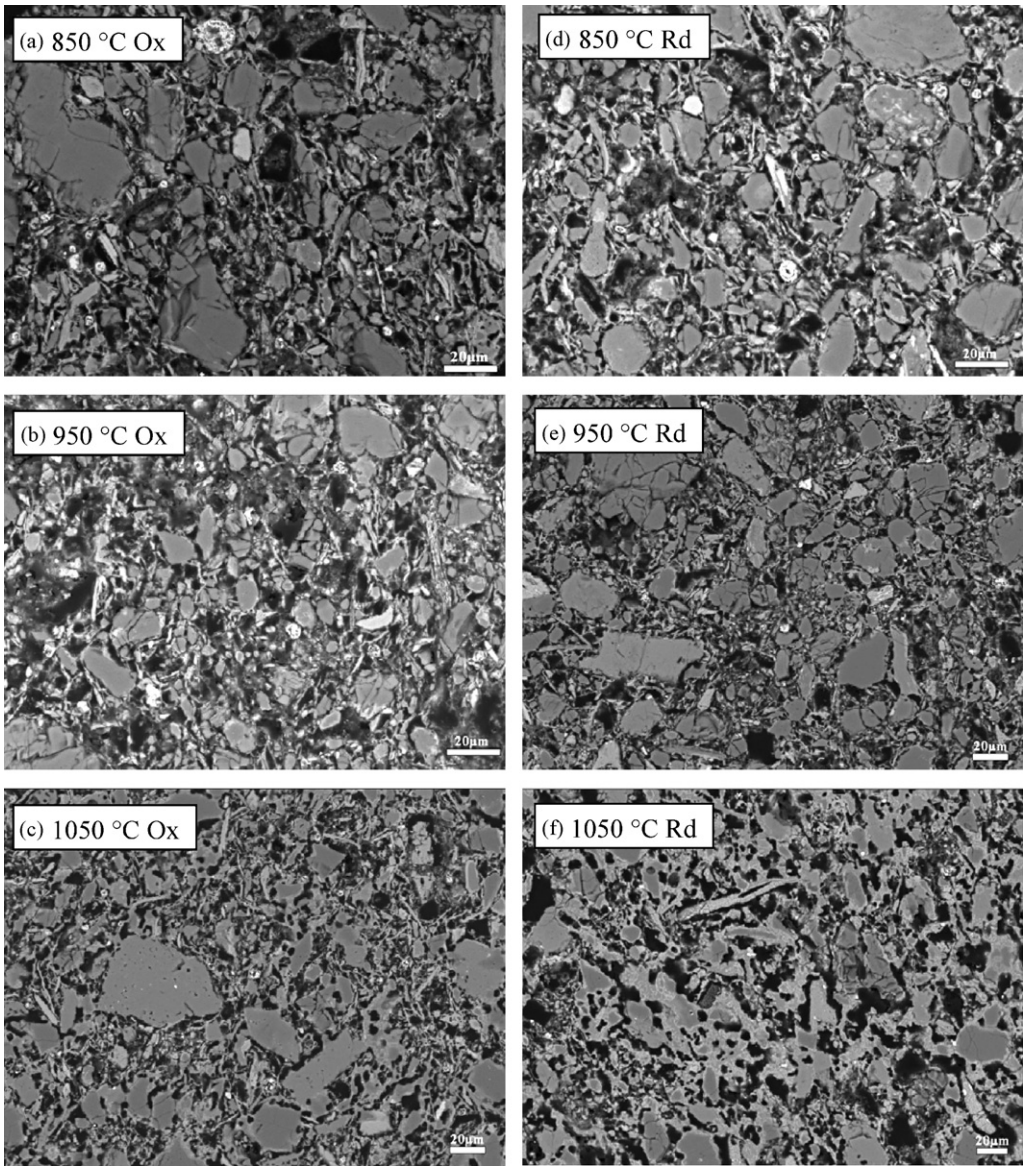

Fig. 3. Backscattered electron images of polished surfaces, after firing TH body in the interval 850–1050 °C, in oxidation (a)–(c) and in reduction (d)–(f).

from 4.3–7.0 wt% at 950 °C to 15.5–20.9 wt% at 1050 °C. Wollastonite, except for TS, and magnetite are further increased compared to 950 °C. The increase of wollastonite and anorthite, in conjunction with the decrease of gehlenite, is in line with the suggested reactions (10) and (11). The higher amount of gehlenite and wollastonite in sample TH was expected as the calcite's content was higher compared to samples G and TS and in addition had a larger medium grain size. The amorphous phase at 1050 °C is expected to be predominantly glassy and ranges between 2.2 and 4.9 wt%.

The colour for both G and TS at 850 and 950 °C is reddish yellow, having a minor difference in hue between the two temperatures (Table 5). For TH the colour is light brown at 850 °C and very pale brown at 950 °C. The crystallisation of fassaite and gehlenite, which permit the entrapment of Fe^{3+} in their crystal structure, limit the formation of hematite and as consequence the red colour. As the temperature rises the colour becomes lighter. The colour at 1050 °C becomes light brown for G and TS and very pale brown for TH. This colour transition is related to the reduction of hematite (red) in the body and the increased formation of magnetite (black) and fassaite (yellow green) (Table 4).

3.2.2. Reducing atmosphere

Firing in a reducing atmosphere at 850 °C leads to a comparable mineralogical assemblage with that for an oxidising atmosphere (Table 4). Quartz, anorthite, albite, sanidine, anorthoclase, fassaite, gehlenite, hematite, magnetite, wollastonite, calcite, white mica and amorphous, are the identified phases by XRD, all levels comparable to that for oxidising atmosphere. Similarly, the microstructure, Figs. 2(d) and 3(d), is comparable to that for an oxidising atmosphere (Figs. 2(a) and 3(a)).

For firings at 950 °C, (Figs. 2(e) and 3(e)), calcite and white mica are no longer present whereas forsterite is the new phase detected. Quartz is decreased. The formation of anorthite is enhanced. Albite increases for G but remains at almost the same levels for TS and TH. Sanidine + anorthoclase, on the other hand, are marginally affected for G but increase for TS and TH. The levels of gehlenite are not affected in G but increase for TS and TH, similarly to the observed trend for an oxidising atmosphere. Levels of fassaite, magnetite and wollastonite are increased; hematite is practically constant. The amorphous content ranges between 5.5 and 6.3 wt%. A comparison of the mineralogical assemblage and microstructure between an oxidising and a reducing atmosphere at 950 °C reveals that the differences are very subtle and therefore the differentiation of the bodies based on these arguments is difficult to be made.

Firing at 1050 °C has a considerable effect on the characteristics of the body. The microstructure is comprised of a network of relatively large, spherical and predominantly closed pores (Figs. 2(f), 3(f) and 4). Compared to an oxidising atmosphere, there is a sharp decrease of quartz levels. Quartz grains are rounded and the diffusion of Si in the matrix has taken place for the quartz grains that are embedded in the body (Fig. 4). As supported by EDS analysis, wollastonite and fassaite have crystallised on the perimeter of quartz grains (Fig. 4). In contrast, quartz grains not in contact with the matrix have practically remained inert, see the upper left grain in Fig. 4. For Ca, higher levels are present in the vicinity of former calcite grains, now present as pores (Fig. 4) Gehlenite and fassaite are usually crystallised in these zones, however gehlenite is drastically reduced compared to 850 and 950 °C as it has started to react with quartz towards wollastonite and anorthite at these firing conditions. The crystallisation of wollastonite along the contact between quartz and gehlenite is also observed. Ca-rich areas, centre of Fig. 4, designate the presence of $Ca(OH)_2/CaCO_3$, which are responsible for the effect of "lime popping/blowing", after hydration and carbonation. The formation of anorthite and fassaite are enhanced and constitute, now, the main crystalline phases. In G and TS, anorthite and fassaite amount together to 50 wt% approximately of the body. In TH, the combined levels are 42 wt% approximately as there is substantial formation of wollastonite, 7.6 wt%, whereas gehlenite, 4.4 wt%, is still present. Wollastonite in G and TS is 2.8 and 6.5wt%, respectively. The smaller content of anorthite and the greater content of wollastonite in sample TH are linked to its greater calcium and lower aluminium content. Sanidine + anorthoclase, detected as grains rich in Si, Al and K in Fig. 4, diminish in all samples as they contribute to the developing of a viscous phase. Glass has been observed to form between quartz and feldspar boundaries. Similarly, magnetite reduces in all samples, unlike albite that is reduced only in G. The behaviour of albite reflects the interplay between two competing trends: an increasing one, as it becomes more An-rich and the overall content rises, and a decreasing one, as it dissolutes in the viscous phase. Al is widespread in the matrix, Fig. 4, although higher levels are present in gehlenite and anorthite. Hematite and forsterite do not show any notable changes in terms of content. The presence of hematite in reducing conditions is attributed to the limited potential of reducing gases to penetrate the body. The levels of Na do not show any topological pattern, in view also of the small initial content, unlike Mg that is usually located in distinct grains (Fig. 4). Typically, there is high coincidence between Mg-rich and Fe-rich grains, which is indicative of former chlorite and mixed-layer clay minerals. Ti is located in distinct grains of ilmenite and rutile (Fig. 4). Even though grains of ilmenite and rutile are present in the raw material, in a number of occasions ilmenite grows as a rim on rutile (Fig. 4). The amorphous phase is notably increased and amounts to 11.2–13.8 wt%. It is predominantly glassy, as suggested by the optical and morphological features (Fig. 3f). As a general comment, the elemental mapping, Fig. 4, corroborates the approach of a heterogeneous system with locally established microsystems.

The colour for both G and TS at 850 °C is reddish yellow (Table 5). For TH the colour is light brown due to the greater amount of fassaite, gehlenite and wollastonite compared to G and TS. As the temperature raises the neocrystallisation increases and the colour becomes gradually lighter. At 1050 °C, TS and TH exhibit the lighter hue in colour, light yellowish brown and pale yellow respectively. However the colour of G becomes slightly darker probably because of the higher amount of magnetite and the lower amount of wollastonite compared to the two others samples.

3.2.3. Comparison between oxidising and reducing atmosphere

In general, the firing behaviour of clays is largely different for oxidising and reducing conditions. Typically, iron under reducing firing, in the form of iron oxides or available after the breakdown of clay minerals, may be incorporated into a vitreous matrix above 800 °C, and crystallise to a variety of Fe^{2+} bearing mineral phases such as olivines (e.g. fayalite Fe_2SiO_4), orthopyroxenes (ferrosilite, $FeSiO_3$), iron-bearing cordierite $[(Mg,Fe)_2Al_4Si_5O_{18}]$, and ferrous mullite in an even higher temperature.[4,44] In the presence of Ca, like in the calcareous clays under study, the breakdown of the initial clay minerals is typically followed by the formation of melilites and clinopyroxenes, which incorporate ferrous and/or ferric ions. That applies for both oxidising and reducing conditions, although, ferric ions prevail in oxidising ones.

In oxidising conditions, the final microstructure comprises an array of calcium-(aluminum,iron)-silicates, such as gehlenite, wollastonite, anorthite and fassaite, which are usually stable between 850 and 1050 °C. In reducing conditions, the formation of viscous phase is more extended and usually the same levels of vitrification are achieved for 50–100 °C less.[4] The difference in the extent of vitrification has been ascribed to the different mineralogical assemblage that prevails depending on the firing atmosphere. In non-calcareous clays, the formation of low melting phases is favoured in reducing conditions, as opposed to oxidising. In calcareous clays, the effect of firing atmosphere is less pronounced. The neomineralisation leads to crystalline phases that exhibit high melting temperature.

In our case, the mineralogy and the microstructure indicate relatively minor differences between oxidising and reducing firing at 850 and 950 °C and become important at 1050 °C. This

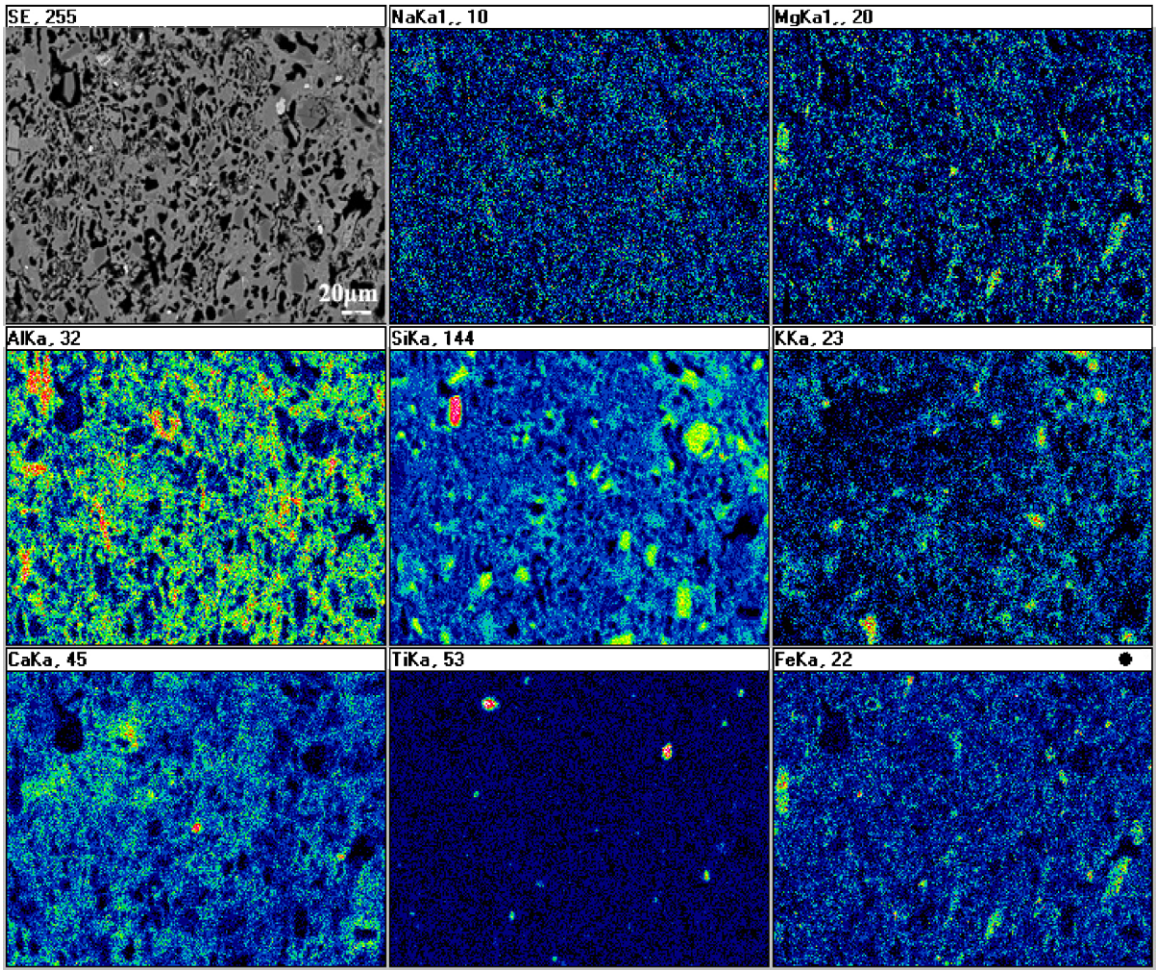

Fig. 4. Elemental mapping of G fired in reducing atmosphere at 1050 °C. Left to right, top row: secondary electrons' image of the surface, Na, Mg, middle row: Al, Si, K, bottom row: Ca, Ti, Fe.

is an outcome of the mild reducing firing atmosphere, as the O_2 concentration is relatively high, the CO_2 levels comparable and only CO differentiates (Table 3). In fact, calcite breakdown has not been delayed in any of the occasions, as one would expect in a CO_2-rich atmosphere compared to a CO_2-poor one. Moreover, EDS and Rietveld analysis reveal that at both atmospheres studied, ferric and ferrous iron co-exist (extensive data are presented in Part II[24]). The latter is in line with the extent of reduction of the Fe_2O_3 powder introduced in the kiln. Magnetite was only formed at 4.7 wt% in reducing atmosphere at 1050 °C. This indicates that the system is marginally at the Fe_3O_4 stability field, of the Fe_2O_3–Fe_3O_4 buffer.

As already commented, the differences become substantial at 1050 °C. Both the crystalline and amorphous phases differ between the oxidising and reducing atmospheres. The higher vitrification is attributed to the role of Fe^{2+}, demonstrated in other studies too.[34,35] Although the prediction of the liquidus of the exact multi-component system does not seem possible in view of the high complexity, it is plausible to suggest that locally established redox reactions led to eutectics, as predicted in the ternary diagrams CaO–FeO–SiO_2 and FeO–Al_2O_3–SiO_2.[45] In addition, low melting phases may have been developed that contribute to liquid phase formation. This is in line with the $CaSiO_3$–$FeSiO_2$ and $CaMgSi_2O_6$–$CaFeSi_2O_6$ binary systems,[46,47] where a clinopyroxene solid solution richer in hedenbergitic component ($CaFeSiO_2$) will convert to wollastonite$_{ss}$, tridymite and liquid, at 1120 °C approximately. As a consequence, the difference in the respective crystalline levels is attributed to two counter-acting phenomena: (a) the dissolution rate of the crystalline compounds in the melt is increased, which subsequently leads to a reduction of the crystals and a change in the properties of the melt (e.g. viscosity and surface tension); (b) the nucleation and growth of the crystals is enhanced, as the mass transfer (i.e. diffusion) is facilitated. Finally, it should be remarked that Fe^{2+} ion in the melt is a network modifier (probably in octahedral coordination) whereas Fe^{3+} is either tetrahedrally or octahedrally coordinated, depending on the ratio $Fe^{3+}/\Sigma Fe$.[48] This differentiation affects the polymerization of the silicate melt[49] and therefore possibly its viscosity as well as the dissolution rate of the solids in the melt. However, as the chemistry of the melt is constantly changing, in view of the concurrent dissolution and crystallisation, and the viscous behaviour of iron-bearing silicate melts is complex,[49] conclusions regarding the effect of the reducing atmosphere on the viscosity of the liquid phase cannot be drawn.

4. Conclusions

The following conclusions are derived:

(a) The effect of the kiln atmosphere for firing at 850 and 950 °C is not intense as the microstructure and mineralogy of the bodies appears to be similar. The body is characterised by open, interconnected porosity whereas the major neo-crystallised minerals are fassaite, gehlenite, anorthite and wollastonite. Difference in colour is observed when fired at 950 °C.
(b) Comparison between the bodies fired at 850 and 950 °C, under a specific firing atmosphere, reveals notable differences in the relative percentages of the mineral phases. Fassaite, gehlenite, anorthite and wollastonite increase, both for oxidising and reducing firing.
(c) For firing at 1050 °C, the differences between the two firing atmospheres become more substantial. The microstructure consists of both open and closed porosity; however in a reducing atmosphere the pores are relatively large, spherical and predominantly closed. Qualitatively the same crystalline phases are present for both firing atmospheres. Anorthite and fassaite constitute the main phases, however, their contents are enhanced in reducing atmosphere.
(d) Higher vitrification has taken place in reducing atmosphere, which is attributed to Fe^{2+} that participates either in the formation of eutectic phases or in low melting crystalline phases.

Acknowledgements

Prof. P. Tsolis-Katagas and Assoc. Prof. G.N. Angelopoulos of University of Patras, are gratefully acknowledged for their support during this work. YP is also thankful to the Research Foundation – Flanders for the post-doctoral fellowship.

References

1. Bauluz B, Mayayo MJ, Yuste A, Fernandez-Nieto C, Gonzalez Lopez JM. TEM study of mineral transformations in fired carbonated clays: relevance to brick making. *Clay Miner* 2004;**39**:333–44.
2. Cultrone G, Rodriguez-Navarro C, Sebastian E, Cazalla O, De La Torre MJ. Carbonate and silicate phase reactions during ceramic firing. *Eur J Miner* 2001;**13**(3):621–34.
3. González-García F, Romero-Acosta V, García-Ramos G, González-Rodríguez M. Firing transformations of mixtures of clays containing illite, kaolinite and calcium carbonate used by ornamental tile industries. *Appl Clay Sci* 1990;**5**(4):361–75.
4. Maniatis Y, Tite MS. Technological examination of Neolithic-Bronze Age pottery from central and southeast Europe and from the Near East. *J Archaeol Sci* 1981;**8**(1):59–76.
5. Nodari L, Marcuz E, Maritan L, Mazzoli C, Russo U. Hematite nucleation and growth in the firing of carbonate-rich clay for pottery production. *J Eur Ceram Soc* 2007;**27**(16):4665–73.
6. Peters T, Iberg R. Mineralogical changes during firing of calcium-rich brick clays. *Am Ceram Soc Bull* 1978;**57**:503–9.
7. Riccardi MP, Messiga B, Duminuco P. An approach to the dynamics of clay firing. *Appl Clay Sci* 1999;**15**(3-4):393–409.
8. Trindade MJ, Dias MI, Coroado J, Rocha F. Mineralogical transformations of calcareous rich clays with firing: A comparative study between calcite and dolomite rich clays from Algarve, Portugal. *Appl Clay Sci* 2009;**42**(3-4):345–55.
9. Moroni B, Conti C. Technological features of Renaissance pottery from Deruta (Umbria, Italy): an experimental study. *Appl Clay Sci* 2006;**33**(3-4):230–46.
10. Noble JV. The technique of attic vase-painting. *Am J Arch* 1960;**64**(4):307–18.
11. Peĭrez JM, Esteve-Teĭbar R. Pigment identification in Greek pottery by Raman microspectroscopy. *Archaeometry* 2004;**46**(4):607–14.
12. Shimada I, Häusler W, Jakob M, Montenegro J, Riederer J, Wagner U. Early pottery making in northern coastal Peru. Part IV: Mössbauer study of ceramics from Huaca Sialupe. *Hyperfine Interact* 2003;**150**(1–4):125–39.
13. Houseman JE, Koenig CJ. Influence of kiln atmospheres in firing structural clay products. I. Maturation and technological properties. *J Am Ceram Soc* 1971;**54**(2):75–82.
14. Houseman JE, Koenig CJ. Influence of kiln atmospheres in firing structural clay products. II. Color development and burnout. *J Am Ceram Soc* 1971;**54**(2):82–9.
15. Maniatis Y, Simopoulos A, Kostikas A, Perdikastis V. Effect of reducing atmosphere on minerals and iron oxides developed in fired clays: the role of Ca. *J Am Ceram Soc* 1983;**66**(11):773–81.
16. Souza GP, Messer PF, Lee WE. Effect of varying quartz particle size and firing atmosphere on densification of Brazilian clay-based stoneware. *J Am Ceram Soc* 2006;**89**(6):1993–2002.
17. Maritan L, Nodari L, Mazzoli C, Milano A, Russo U. Influence of firing conditions on ceramic products: experimental study on clay rich in organic matter. *Appl Clay Sci* 2006;**31**(1-2):1–15.
18. Denissen JAM. Reduction firing of building ceramics. Part I. *Ziegelindustrie Int/Brick Tile Indus Int* 1993;**46**(10):636–42.
19. Hauck D, Kruetzner-Brezynski B, Ruppik M. Different firing chamber atmospheres for improvement of product properties. *Ziegelindustrie Int/Brick Tile Indus Int* 1995;**11**:851–9.
20. Petropoulos M. *Roman lamp workshops at Patras and the Lychnomanteion, vol. 70. Archaeol. Bulletin*. Athens, Greece: Ministry of Cultural Heritage; 1999.
21. Rathossi C. Ancient ceramics from NW Peloponnese and the provenance of their raw materials: a petrographic, mineralogical, geochemical and archaeometric approach. PhD thesis, University of Patras, Patras; 2005.
22. Rathossi C, Tsolis-Katagas P, Katagas C. Technology and composition of Roman pottery in northwestern Peloponnese, Greece. *Appl Clay Sci* 2004;**24**(3-4):313–26.
23. Rathossi C, Katagas C, Tsoli-Katagas P. Major and trace element characterization of Archaic and Roman pottery from Achaia, Greece. In: Isabel Prudêncio M, Isabel Dias M, Waerenborgh JC, editors. *Understanding people through their pottery, 7th European meeting on ancient ceramic (EMAC'03)*. 2003.
24. Rathossi C, Pontikes Y. Effect of firing temperature and atmosphere on ceramics made of NW Peloponnese clay sediments: Part II. Chemistry of pyrometamorphic minerals and comparison with ancient ceramics. *J Eur Ceram Soc* 2010;**30**(9):1853–66.
25. Jackson ML. *Soil chemical analysis—advanced course*. University of Wisconsin-Madison Libraries; 1974.
26. Zervas E. Formation of oxygenated compounds (aldehydes, alcohols, organic acids) from propane flames. *Environ Eng Sci* 2005;**22**(5):651–9.
27. Hasaki E. Ceramic kilns in ancient Greece: technology and organization of ceramic workshops. PhD dissertation, University of Cincinnati; 2002.
28. Jauhiainen J, Martin-Gullon I, Conesa JA, Font R. Emissions from pyrolysis and combustion of olive oil solid waste. *J Anal Appl Pyrolysis* 2005;**74**(1-2):512–7.
29. Bish DL, Post JE. Quantitative mineralogical analysis using the Rietveld full-pattern fitting method. *Am Miner* 1993;**78**(9-10):932–40.
30. Veniale F. Raw material and manufacturing processes in ancient ceramic artefacts. In: Burragato F, Grubessi O, Lazzarini L, editors. *Proceedings of the 1st European workshop on archaeological ceramics*. 1994. p. 55–72.
31. Greenwood HJ. Wollastonite: stability in HO–CO mixtures and occurrence in a contact-metamorphic aureole near Salmo, British Columbia, Canada. *Am Miner* 1967;**52**:1669–80.

32. Hewitt DA. The metamorphism of micaceous limestones from south-central Connecticut. *Am J Sci* 1973;**273 A**:444–69.
33. Kerrick DM. *Contact metamorphism*, vol. 26. Mineralogical Society of America; 1991. p. 210–1.
34. Pontikes Y, Angelopoulos GN. Effect of firing atmosphere and soaking time on heavy clay ceramics with addition of Bayer's process bauxite residue. *Adv Appl Ceram* 2009;**108**(1):50–6.
35. Pontikes Y, Rathossi C, Nikolopoulos P, Angelopoulos GN, Jayaseelan DD, Lee WE. Effect of firing temperature and atmosphere on sintering of ceramics made from Bayer process bauxite residue. *Ceram Int* 2009;**35**(1): 401–7.
36. Vedder W, Wilkins RWT. Dehydroxylation and rehydroxylation, oxidation and reduction of mica. *Am Miner* 1969;**54**(3-4):482–509.
37. Grapes RH. *Pyrometamorphism*. Springer; 2006.
38. Rice JM. Contact metamorphism of impure dolomitic limestone in the Boulder Aureole, Montana. *Contrib Miner Petrol* 1977;**59**(3): 237–59.
39. Dondi M, Ercolani G, Fabbri B, Marsigli M. Chemical composition of melilite formed during the firing of carbonate-rich and iron-containing ceramic bodies. *J Am Ceram Soc* 1999;**82**(2):465–8.
40. Dondi M, Ercolani G, Fabbri B, Marsigli M. An approach to the chemistry of pyroxenes formed during the firing of Ca-rich silicate ceramics. *Clay Miner* 1998;**33**(2-3):443–52.
41. Stepkowska ET, Jefferis SA. Influence of microstructure on firing colour of clays. *Appl Clay Sci* 1992;**6**:319–42.
42. Duminuco P, Messiga B, Riccardi MP. Firing process of natural clays. Some microtextures and related phase compositions. *Thermochim Acta* 1998;**321**(1-2):185–90.
43. Veniale F. Modern techniques of analysis applied to ancient ceramics. *Adv Workshop Anal Methodologies Investig Damaged Stones* 1990:1–45.
44. Wagner FE, Wagner U. Mössbauer spectra of clays and ceramics. *Hyperfine Interact* 2004;**154**(1-4):35–82.
45. The American Ceramic Society. *Phase diagrams for ceramists, vol. I*. Columbus (OH): The American Ceramic Society; 1964.
46. Bowen NL, Schairer JF, Posnjak E. The system, CaO–FeO–SiO_2. *Am J Sci* 1933;**26**:193–284.
47. Schairer JF, Yoder Jr HS. The system diopside-enstatite-silica. *Carnegie Inst Wash, Yearb* 1962;**61**:75–82.
48. Mysen BO, Virgo D, Neumann ER, Seifert FA. Redox equilibria and the structural states of ferric and ferrous iron in melts in the system CaO–MgO–Al_2O_3–SiO_2–Fe–O: relationships between redox equilibria, melt structure and liquidus phase equilibria. *Am Miner* 1985;**70**(3-4):317–31.
49. Mysen BO, Virgo D, Scarfe CM, Cronin DJ. Viscosity and structure of iron- and aluminum-bearing calcium silicate melts at 1 atm. *Am Miner* 1985;**70**(5-6):487–98.